https://doi.org/10.5194/egusphere-2026-1635
Preprint. Discussion started: 8 April 2026

Spatiotemporal dynamics of shear stress partitioning around vegetation in a sparsely vegetated dryland

Pei Zhang[1], Brandon L. Edwards[1], John A. Gillies[2], George Nikolich[2], Andrew Trautz[3], Brandi Wheeler[1], Nancy P. Ziegler[3]

[1]Jornada Experimental Range, New Mexico State University, Las Cruces, NM, USA.
[2]Division of Atmospheric Sciences, Desert Research Institute, Reno, NV, USA.
[3]US Army Corps of Engineers ERDC, Vicksburg, MS, USA.

Correspondence to: Pei Zhang (peizhang@nmsu.edu)

Keywords: wind erosion, surface shear stress, drag partitioning, shrubland

Abstract. Vegetation is the dominant regulator of wind erosion and dust emission in drylands. Drag partition theory is typically used to quantify how vegetation reduces surface shear stress, but lateral flow acceleration along plant sides and the resulting spatiotemporal patterns of shear stress redistribution around individual plants in the field remain understudied. Here we quantify the surface shear stress ratio, its spatial and temporal variability, and lateral flow acceleration along the side of a shrub across a range of wind magnitudes and phenological phases. The spatial variability of the surface shear stress ratio exceeded that reported previously, whereas the temporal variability was 75 % of the spatial variability. Along the shrub side, surface shear stress ratio was independent of wind speed and exhibited a statistically significant decreasing trend with foliar growth while maintaining pronounced spatial heterogeneity, including localized shear amplification near shrub margins. The shape and position of the acceleration zone was broadly consistent with prior studies, although uncertainties remain regarding how vegetation type and dimensional traits influence its extent and form. Incorporating phenology-dependent, yet wind speed-independent, shear stress redistribution and spatiotemporal variability into drag partition schemes provides a pathway toward improved process-based representation of vegetation-wind interactions in wind erosion models. This refinement could improve predictions of the timing, location, magnitude, and frequency of aeolian sediment transport and dust emission, including low-intensity events when above-canopy winds are near or below conventional thresholds.

Graphical abstract

https://doi.org/10.5194/egusphere-2026-1635
Preprint. Discussion started: 8 April 2026

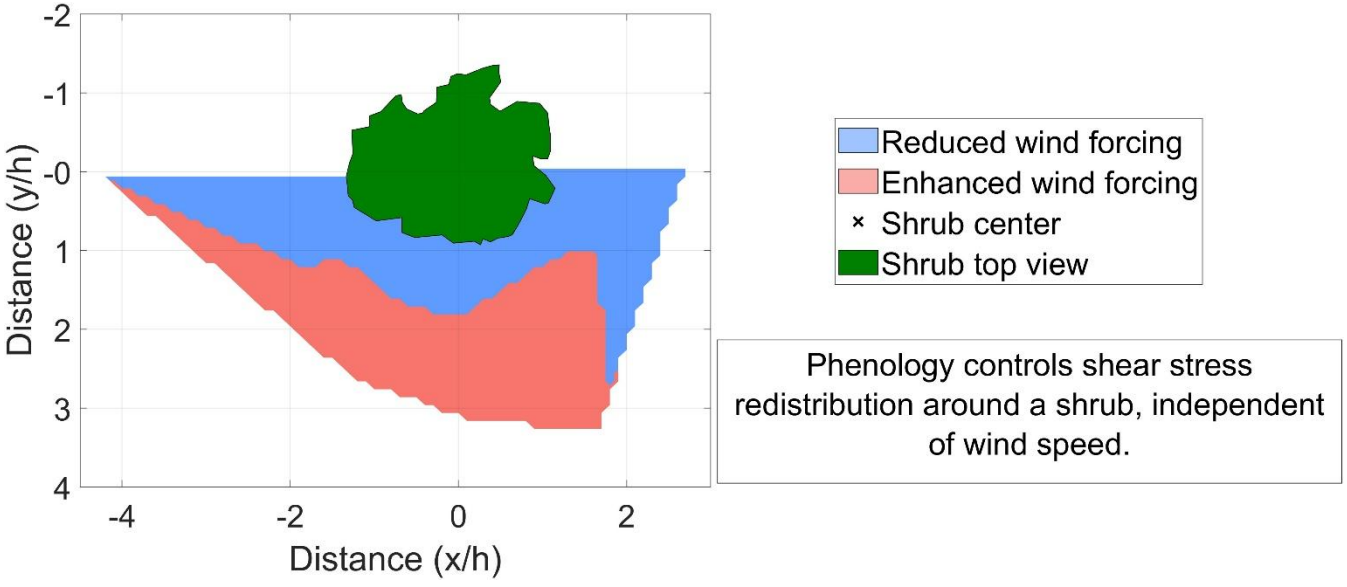

1 Introduction

Vegetation is a first-order control on wind erosion and dust emission—it directly influences the spatial distribution of wind shear velocity at the soil surface (u_{*s}, m s^{-1}) that initiates and sustains aeolian sediment transport (Duniway et al., 2019; Dupont et al., 2014; Okin, 2008; Raupach et al., 1993). Drag partition theory is typically used to describe vegetation-fluid interactions by representing reductions in surface shear stress that result from momentum extraction and aerodynamic sheltering, thereby reducing wind erosivity and protecting the soil surface from erosion (Okin, 2008; Raupach, 1992; Raupach et al., 1993). However, flow around vegetation also increases local wind speed (U, m s^{-1}) and u_{*s} along the sides of individual plants (de Langre, 2008; Leenders et al., 2007; Mayaud et al., 2016a; Miri & Webb, 2022; Shaw, 1977; Wolfe & Nickling, 1993). Such accelerations can enhance aeolian sediment transport around vegetation even though the soil surface remains aerodynamically sheltered downwind; sediment transport and dust emission can subsequently occur when above-canopy wind speeds at or below transport thresholds (Bergametti and Gillette, 2010; Fu et al., 2019; Gillette et al., 2006; Hong et al., 2020; Judd et al., 1996; King et al., 2005; Li et al., 2008; McKenna Neuman and Bédard, 2015; Wolfe and Nickling, 1993). Despite the influence of vegetation on lateral wind speed being well recognized (Ash & Wasson, 1983; Cheng et al., 2019; Leenders et al., 2007; Li et al., 2008; Miri & Webb, 2022; Shaw, 1977; Wolfe & Nickling, 1993), few studies have quantified the spatial distribution of u_{*s} around individual plants in natural environments. This limits both our current understanding of wind erosion and ability to accurately predict dust emissions in sparsely vegetated landscapes.

https://doi.org/10.5194/egusphere-2026-1635
Preprint. Discussion started: 8 April 2026

In near-surface airflow over vegetated surfaces, three characteristic flow zones associated with individual plants are commonly observed: 1) an upstream deceleration zone; 2) a shelter or wake zone downstream; and 3) lateral acceleration zones along both sides. Ash and Wasson (1983) reported wind speed increases of up to 130 % around dunefield shrubs measured with a handheld anemometer at an unspecified height and qualitatively delineated an acceleration zone showing an arcuate elliptical shape. Subsequent studies (Leenders et al., 2007; Sutton and Mckenna Neuman, 2008; Cheng et al., 2019; Fu et al., 2019) similarly observed that lateral wind speed increased by 105 %-167 % at heights ranging from 0.05× of the canopy height to equal the canopy height and found that acceleration zones exhibited an elliptical shape that varied in size and position relative to the plant. Sutton and McKenna Neuman (2008) showed that increases in lateral surface shear stress and its distribution appeared to vary with wind speed (cf. Fig. 9a–c). In wind tunnel experiments, Cheng et al. (2019) found that lateral wind speed acceleration typically ranged from 105 % to 110 %, rarely exceeding 115 %, and the acceleration zone size decreased with increasing wind speed. Using numerical simulation, Fu et al. (2019) demonstrated that acceleration effects were strongly influenced by basal shape, with maximum increases in wind speed ranging from 138 % to 167 %—higher than previous findings. They attributed these differences to wind speed observation height, element geometry, and porosity; they specifically recommended further investigation into the influence of vegetation porosity and wind direction. Field experiments have reported somewhat lower acceleration effects. Leenders et al. (2007) found average increases of 106 % at the side of two shrubs (0.6 m high) with wind speed measured at 0.4 m height, while Miri and Webb (2022) observed a 104–130 % increase around a 1.5 m tall *Tamarix* shrub at a measurement height of 0.75 m.

In sparsely vegetated drylands, unobstructed transport corridors—such as vegetation gaps or wind streets—are often preferentially aligned with the dominant wind direction (Gillette et al., 2006; King et al., 2006; Mayaud et al., 2016a; Mayaud & Webb, 2017; Okin & Gillette, 2001; Ziegler et al., 2023), forming vegetation-interspace mosaic landscapes. As intercanopy gaps and wind streets develop, acceleration zones associated with individual plants can coalesce, effectively expanding the area of soil surface exposed to intensified wind erosion. This leads to deflation, nutrient removal, and damage to intercanopy vegetation (Payne et al., 2023), thereby accelerating further land degradation. For example, Webb et al. (2025) demonstrated how loss of herbaceous grass cover within shrub interspaces in a Chihuahuan Desert shrubland, led to increased connectivity of bare surfaces, larger wind erosion magnitude, and increased variability in observed transport rates.

The amount of turbulent energy reaching the surface, i.e., u_{*s}, is the key driver of wind erosion and dust emission, but estimates of acceleration and sheltering based solely on height-dependent wind speed measurements can yield substantial differences in u_{*s}. For example, both Fu et al. (2019) (cf. Fig. 3) and Cheng et al. (2019) (cf. Fig. 7) demonstrated that wind speed acceleration is stronger closer to the surface, highlighting the need to directly quantify lateral increases in u_{*s}. Ziegler et al. (2023) demonstrated that both the average ratio of u_{*s} to shear velocity (u_*, m s^{-1}) and its spatial variability were directly linked to vegetation phenological transitions from dormant to leaf-on conditions. Further, observed large spatial variability in sediment transport rates provides strong evidence for substantial differences in u_{*s} across sparsely vegetated rangelands (e.g., Chappell et al., 2003; Sterk et al., 2004; Webb et al., 2019; Wojcikiewicz et al., 2023), which underscores the need to quantify the distribution of u_{*s} around individual vegetation elements.

https://doi.org/10.5194/egusphere-2026-1635
Preprint. Discussion started: 8 April 2026

Despite advances in instrumentation and numerical modeling, a critical gap remains in the direct, spatially explicit field measurement of u_{*_s} around vegetation. The limited number of studies on u_{*_s} in field environments can be attributed to several factors including, the difficulty of accurately estimating u_{*_s} from height-dependent wind speed measurements (Baas, 2019; Bauer et al., 2013; King et al., 2008; Kunadi et al., 2024; Lee and Baas, 2016); the complexity of near-surface airflow beneath the canopy (Breshears et al., 2009; Mayaud & Webb, 2017); limitations in instrument size and efficiency for high-resolution spatial measurements (Bauer et al., 2022); and the dynamic changes in vegetation porosity, morphology, and flexibility associated with phenological transitions (Fu, 2019; Fu et al., 2019; Miri et al., 2017, 2018; Suter-Burri et al., 2013; Walter et al., 2012; Ziegler et al., 2023). This study quantifies the spatiotemporal dynamics of u_{*_s} and compares the response of drag partitioning (shear stress redistribution) to vegetation phenology and wind forcing along the side of a shrub-interspace mosaic in a sparsely vegetated dryland. We used up to 18 wireless Irwin sensors to measure u_{*_s} around a *Prosopis glandulosa* Torr. (honey mesquite) shrub. Specifically, we analyzed whether drag partitioning is dependent on wind forcing or on vegetation phenology. Our results show that the surface shear stress ratio (R': normalized u_{*_s}) is independent of wind speed; however, the average of R' shows a statistically significant decreasing trend across phenological phases while maintaining pronounced spatial heterogeneity, including localized shear amplification near shrub margins. We further delineated the shape and position of the zone with enhanced u_{*_s}, which is broadly consistent with previous studies, but uncertainties remain regarding how vegetation type and plant morphological traits influence its extent and shape.

2 Methods

2.1 Study site and data collection

Field experiments were conducted at a National Wind Erosion Research Network (Webb et al., 2016) site at the USDA-ARS Jornada Experimental Range (https://winderosionnetwork.org) in the northern Chihuahuan Desert, New Mexico, USA (32.6271°N, 106.7387°W, ~1320 m AMSL). Vegetation at the site is dominated by honey mesquite shrubs (*Prosopis glandulosa* Torr.) but also includes several species of forbs and warm season (C4) grasses. The surface slope is less than 0.5 % and the surface soil texture is loamy sand with weak biological and physical crusting.

Wireless Irwin sensors were used to quantify u_{*_s} (Ziegler et al., 2026). These sensors are a newer version of the design of Gillies et al. (2006, 2007) and were deployed adjacent to a ~1 m tall mesquite shrub from 2 February to 7 July 2023 and from 12 February to 20 June 2024. The Irwin sensors were installed flush with the ground surface with all electronics located in a subsurface housing. Their output was sampled at a frequency of 1 Hz. Ten sensor locations were installed in 2023 with an additional eight locations added in 2024. Their positions were recorded using a Trimble Geo XH 6000 unit, with a mean horizontal error of 19 cm. Sensor locations were selected to capture the spatial patterns of u_{*_s} around the shrub perpendicular to the dominant wind direction (Fig. 1). The fetch length to the nearest upwind shrub in the dominant wind direction was ~15 m, with scattered grasses and forbs along the fetch. Sensors were removed about once per week for routine cleaning and battery recharging.

https://doi.org/10.5194/egusphere-2026-1635
Preprint. Discussion started: 8 April 2026

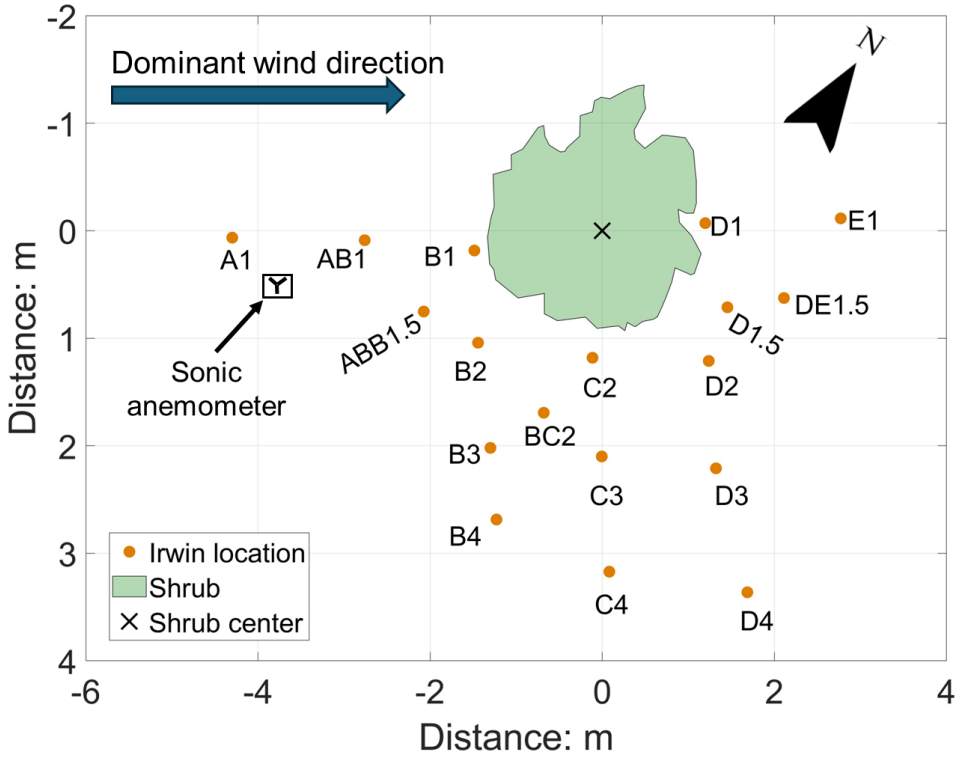

Figure 1. Instrument deployment at the study site (plan view). Three rows (B, C, and D rows) are about perpendicular to the dominant wind direction. The height of the shrub is about 1 meter. The 3-D sonic anemometer is installed 1 m above the surface.

A Gill WindMaster 3-D sonic anemometer was installed ~3 m upwind of the shrub to continuously measure the wind vector at 1 m height above the soil surface (Fig. 1). The anemometer was sampled at 20 Hz. We used PhenoCam data (PhenoCam Network, 2024) collected between February and July of 2023 and 2024 to quantify seasonal vegetation phenology (Richardson et al., 2018). Following Ziegler et al. (2023), the three-day average Green Chromatic Coordinate metric (G_{CC}) and field site photos (Figs. 2 & 3), were used to identify three plant phenology phases: dormant, green-up, and leaf-on. The Green Chromatic Coordinate (G_{CC}) is a derived metric from PhenoCam imagery ($0 \leq G_{CC} \leq 1$) that represents the relative greenness of vegetation within the defined region of interest.

https://doi.org/10.5194/egusphere-2026-1635
Preprint. Discussion started: 8 April 2026

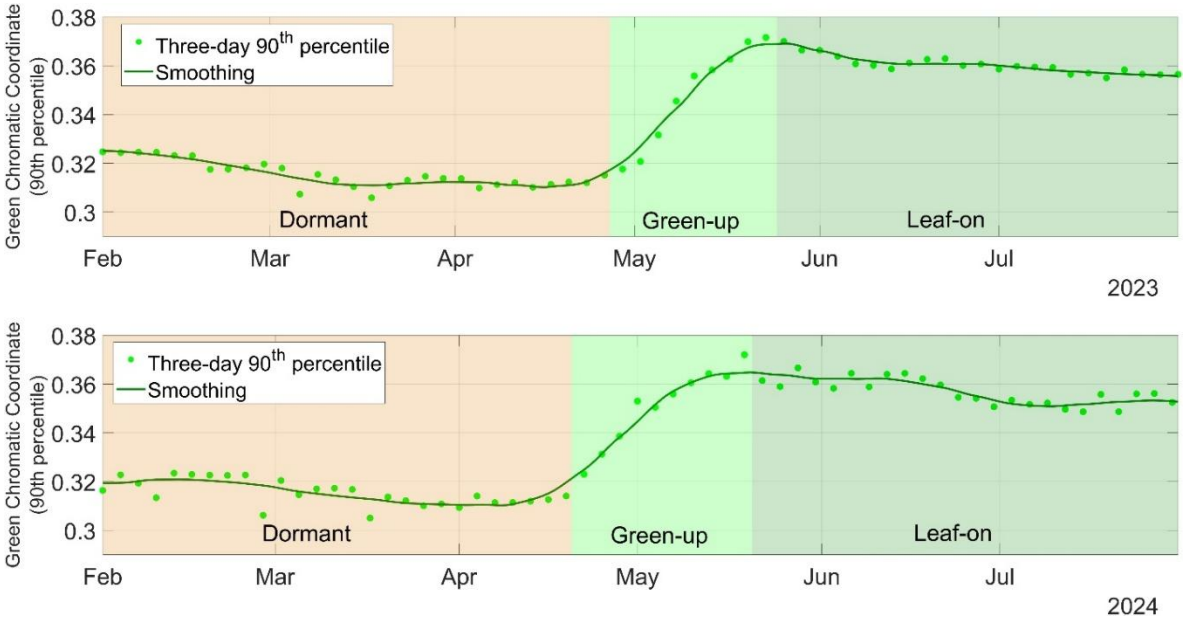

125 Figure 2. Time series of the three-day 90th percentile Green Chromatic Coordinate (G_{CC}) from the study site during the data collection periods. Phenological phases are labeled in different shaded color boxes.

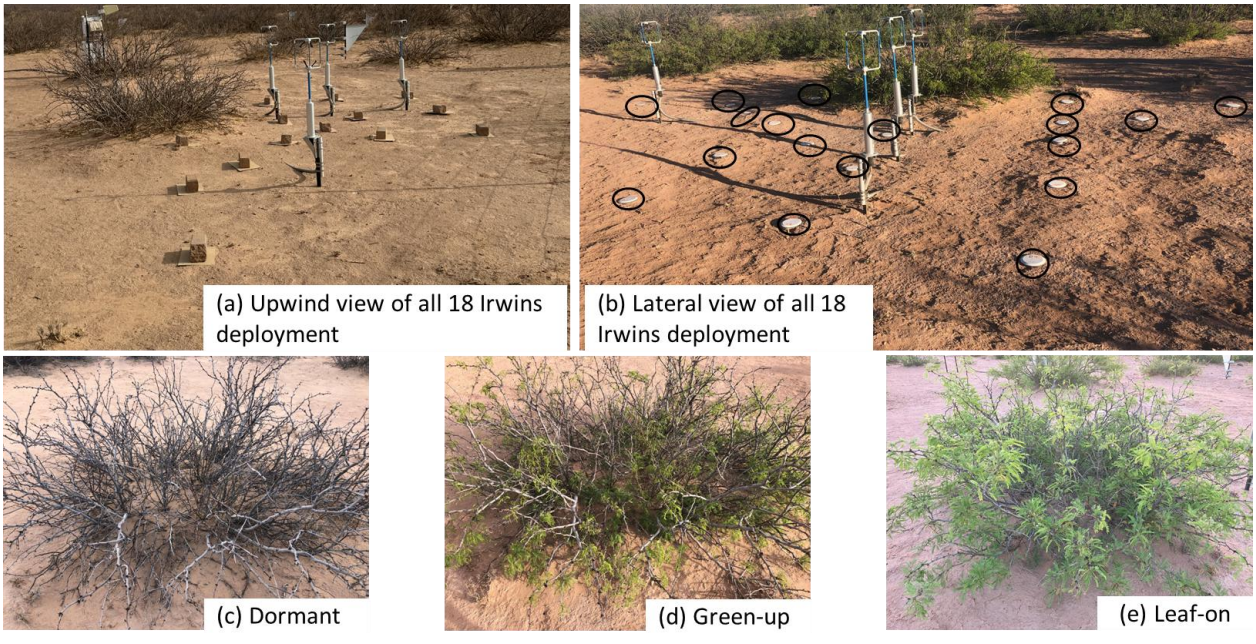

Figure 3. Instrument setup and site photos across three phenological phases. (a) Overview photo of the study site taken on
130 January 6, 2025, facing downwind of the dominant wind. (b) Lateral view of all 18 installed Irwins. The black circles highlighted the locations of 18 Irwins. The photo was taken on April 30, 2024. Note: data from the three sonic anemometers

https://doi.org/10.5194/egusphere-2026-1635
Preprint. Discussion started: 8 April 2026

shown in panels (a) and (b) and positioned along the side of the shrub were not included in this analysis. (c) Photo taken during the dormant phase on March 8, 2024. (d) Photo taken during the green-up phase on April 24, 2024. (e) Photo taken during the leaf-on phase on May 23, 2024.

2.2 Estimating surface shear velocity

The Irwin sensors were calibrated using the wind tunnel at the U.S. Army Engineer Research and Development Center (ERDC) Synthetic Environment for Near-Surface Sensing and Experimentation (SENSE) research facility and a PI-SWERL portable field laboratory. Wind tunnel calibration was limited to a relatively narrow range of u_{*s} (< 0.4 m s^{-1}). Therefore, PI-SWERL (Etyemezian et al., 2014) experiments were conducted to extend the calibration to higher shear velocities representative of field conditions. Shear velocity during wind tunnel tests was estimated from vertical wind speed profiles with laser Doppler anemometers. Shear velocity during the PI-SWERL tests was estimated following Etyemezian et al. (2014) and Ziegler et al. (2023). A power law was fitted to relate differential pressure (Δp) measured by the sensors to u_{*s}:

$$u_{*s} = 0.1610 \times \Delta p^{0.3755} \quad (1)$$

R^2=0.99, RMSE = 0.024, p < 0.001, N=193

based on all calibration data from both wind tunnel and PI-SWERL experiments (Fig. 4). Equation 1 was applied to all sensors.

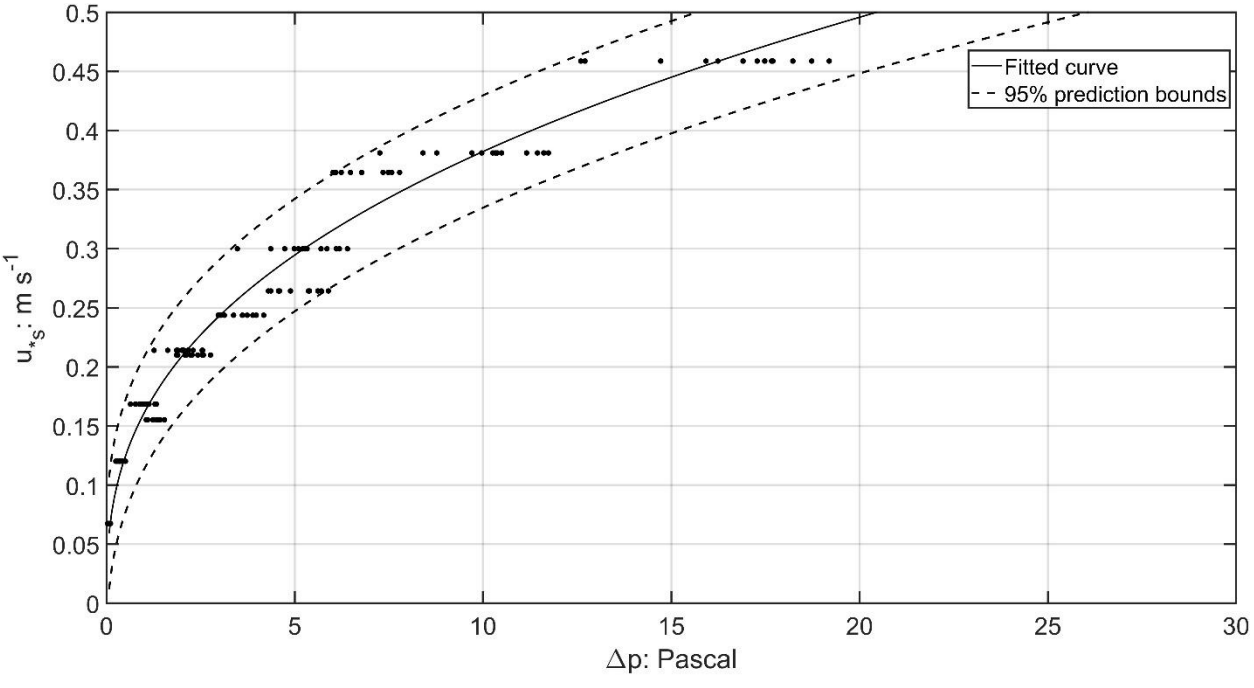

Figure 4. Calibration curve and 95 % prediction bounds for Irwin sensors including all samples in wind tunnel and PI-SWERL.

https://doi.org/10.5194/egusphere-2026-1635
Preprint. Discussion started: 8 April 2026

The datasets collected from the Irwin sensors and the sonic anemometer were filtered to retain only periods when the wind speed (U, m s^{-1}) measured at a height of 1 m exceeded 4 m s^{-1}. This threshold was selected based on the 5-minute averaging interval and 1 m measurement height to minimize low-frequency loss in shear velocity (u_*, m s^{-1}) estimation, following van Boxel et al. (Fig. 3 2004). High-frequency loss may occur at high wind speeds (>10 m s^{-1}) based on spectral analyses in Figs 4 and 5 of van Boxel et al. (2004). Such wind speeds occurred only during 2024 and accounted for about 2 % of the total samples. The data analyzed was further restricted to when the wind blew from the dominant direction (225° ± 30°) which corresponds to flow approximately perpendicular to the Irwin deployment. Following the double-rotation method of Zhang et al. (2024), u_* was estimated using wind vector measurements obtained with the sonic anemometer positioned about 3 meters upwind of the shrub (Fig. 1). Both u_* and u_{*_s} were restricted to periods when wind direction fell within the dominant sector (225° ± 30°), corresponding approximately to flow perpendicular to the Irwin sensor deployment, and were both estimated over 5-minute intervals.

2.3 Shear stress ratio and erosivity

Raupach et al. (1993) defined drag partitioning between roughness elements and the soil surface as the ratio of shear stress at the soil surface to total shear stress over the landscape. To quantify the impact of the shrub on shear stress redistribution, we estimated the surface shear stress ratio (R') following their formulation as:

$$R' = u_{*s}/u_* \quad (2)$$

where u_{*s} is the average surface shear velocity at each location within a 5-min interval estimated from the Irwin sensors, and u_* is the turbulent shear velocity for the corresponding period estimated from the sonic anemometer. The maximum shear stress ratio (R'') was calculated as:

$$R'' = u_{*s\,max}/u_* \quad (3)$$

where $u_{*s\,max}$ is the maximum surface shear velocity within the same 5-minute interval at each location.

We compared temporal variability of the shear stress ratio using simple linear regression between R' and R'' for each location separately, using all 5-min samples within each phenological phase, following King et al. (2006). This resulted in up to 18 fitted slopes per phenological phase, each representing the temporal sensitivity of R'' to R' at an individual location. Similarly, spatial variability was compared using simple linear regression between the spatial average of R' and the corresponding spatial maximum R'' across all locations, using all 5-min samples within each phenological phase.

Erosivity (e) was defined as the R' normalized to reference location A1 (Fig. 1), where u_{*_s} is assumed to be minimally influenced by the shrub. If $e > 1$, the location is expected to experience fluid acceleration, indicating greater erosivity potential than the bare surface at the reference location. Conversely, if $e < 1$, the location is considered sheltered. The boundary between sheltering and acceleration zones is defined as $e = 1$. Variation in the separation line across phenological phases was examined to assess vegetation effects on sheltering and acceleration.

https://doi.org/10.5194/egusphere-2026-1635
Preprint. Discussion started: 8 April 2026

Estimates of shear stress ratio features for Eqs. 2–3 were filtered to reduce potential sample location bias. Because of external issues or user error during data collection (e.g., sediment burial, insect intrusion in pressure tubing, battery depletion, or loose wiring), not all time periods contained useable data from the same set of sensors. Therefore, we filtered the data to require that 8, 10, and 18 sensors were functioning simultaneously during 2023, the dormant phase of 2024, and the remainder of 2024, respectively. Estimates of erosivity (e) were additionally filtered to a narrower wind direction range of 245 ±10°, as any bias from wind direction at the reference location (A1, Fig. 1) could be amplified in the subsequent analysis. The spatial distribution of R' and e around the shrub was visualized by linear interpolation onto a 10 cm grid using the MATLAB function *griddata*. Linear interpolation provides a conservative representation of the measured spatial patterns without imposing additional smoothing or model-dependent structure. The spatial distributions of R' and e along the x- and y axes around the shrub were normalized by shrub height (h).

2.4 Wind speed and phenology

Simple linear regression analysis was used to examine the relationship between R' and horizontal wind speed (U, m s^{-1}) at 1 m height for each phenological phase and year. The samples of R' were grouped into three phenological phases based on G_{CC} (Fig. 2). The Mann-Kendall trend tests (Burkey, 2020) were used to evaluate if there were statistically significant (p-value < 0.05) trends in U, u_*, R', and R'' through the phenological phases.

3 Results

Three phenological phases were identified based on the three-day average G_{CC} and field site photographs (Figs. 2 & 3): dormant (February 14–April 26, 2023; February 12–April 19, 2024), green-up (April 27–May 23, 2023; April 20–May 19, 2024), and leaf-on (May 24–July 7, 2023; May 20–June 20, 2024). After filtering for location bias, 706, 87, and 477 samples remained for the dormant, green-up, and leaf-on phases, respectively, in 2023, and 804, 182, and 443 samples remained for the corresponding phases in 2024 (Zhang et al., 2025).

3.1 Spatiotemporal characteristics of shear stress ratio

The Mann-Kendall trend test ($p < 0.05$) indicated a statistically significant decrease trend in the mean values of both R' and R'' across phenological phases (Fig. 5). The spatially maximum R'' decreased in 2023 but increased in 2024 across phenological phases (Fig. 5). Shear velocity (u_*) showed no trend in 2023 but exhibited a mild decrease trend in 2024. In contrast, wind speed measured at 1 meter height showed a statistically significant decrease trend across phenological phases in both years (Fig. 6).

https://doi.org/10.5194/egusphere-2026-1635
Preprint. Discussion started: 8 April 2026

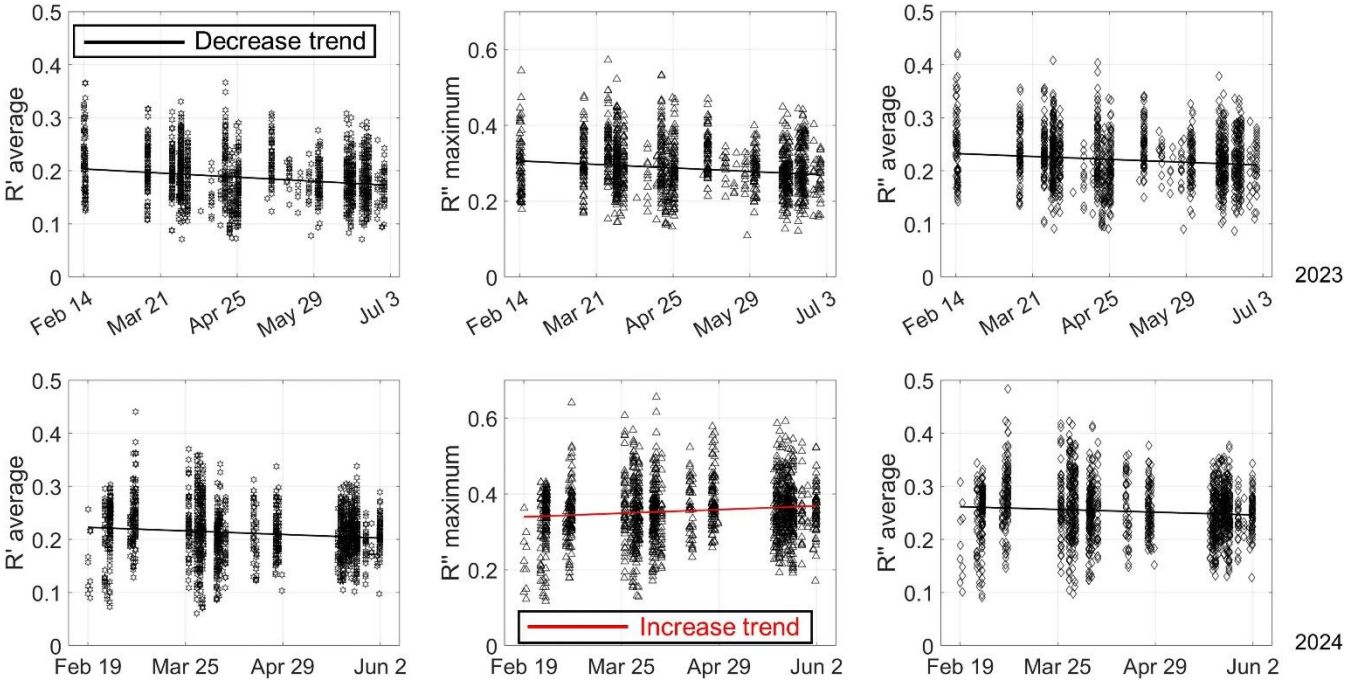

Figure 5. Spatiotemporal trends of the shear stress ratio across phenological phases. The black lines show statistically significant decrease ($p<0.05$) trends, and the red lines indicate statistically significant increase trends, based on the Mann-Kendall trend test.

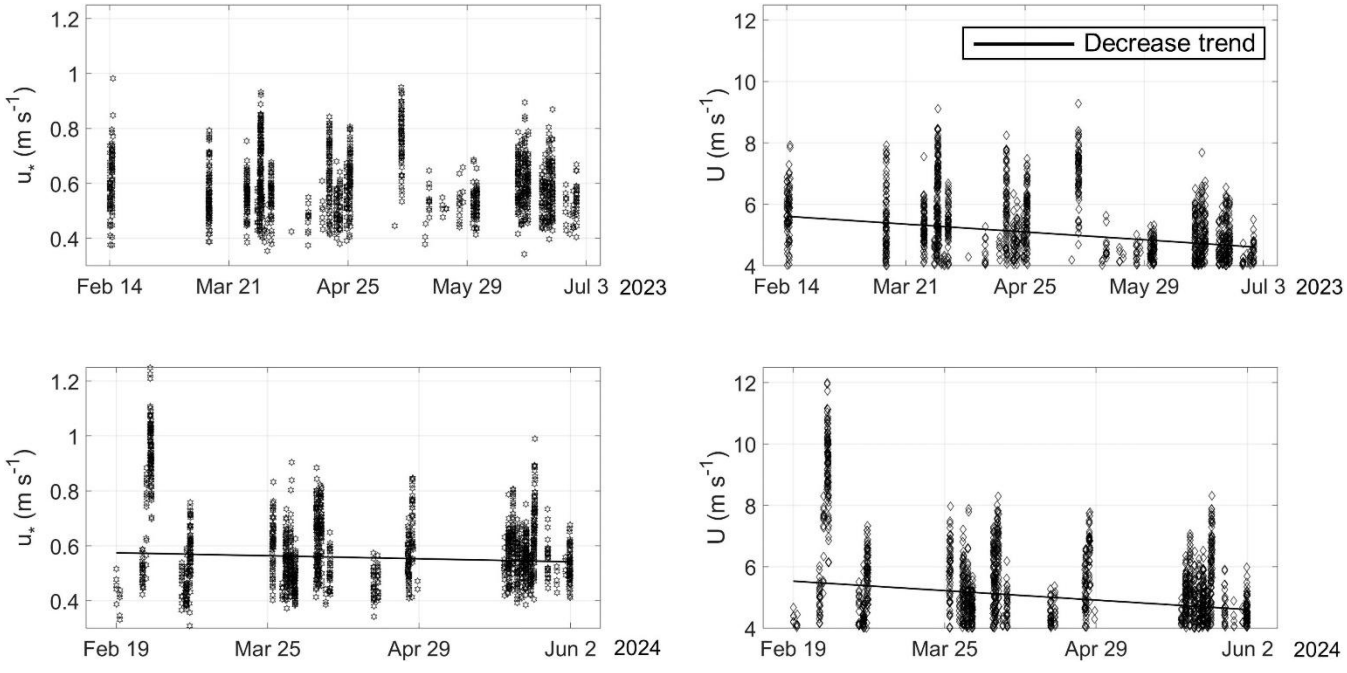

https://doi.org/10.5194/egusphere-2026-1635
Preprint. Discussion started: 8 April 2026

Figure 6. Wind forcing trends across phenological phases. The black lines indicate statistically significant decrease ($p<0.05$) trends based on the Mann-Kendall trend test.

A strong relationship was found between the spatial average of R' and the corresponding spatial maximum R'' across all locations in both years (Fig. 7): $Y = 1.53 \times X, R^2 = 0.85, p < 0.05$ in 2023 and $Y = 1.63 \times X, R^2 = 0.71, p < 0.05$ in 2024. The fitted slope value was significantly higher ($p < 0.05$, 6.5 %) in 2024 than in 2023. Phenological phase-specific regressions showed that variation in the spatial variability of shear stress ratio relative to the annual trend was <3 % in 2023 and <10 % in 2024 (Table 1). The highest fitted slope (1.78) was during the green-up phase in 2024, whereas in 2023, it was approximately equal during the dormant and leaf-on phases. On average, the spatial variability of shear stress ratio was 1.9 %, 16.29 %, and 11.1 % higher in 2024 than in 2023 during the dormant, green-up, and leaf-on phases, respectively.

Table 1. Spatiotemporal characteristics of the shear stress ratio across vegetation phenological phases in 2023 and 2024

Phase	N	Spatial variability (slope coefficient)	R^2	Temporal variability (slope coefficient)	R^2
Annual 2023	1270	1.53^{a}	0.85	1.17	0.93
Dormant 2023	706	1.53^{Aa}	0.84	1.16	0.94
Green-up 2023	87	1.49^{Ba}	0.86	1.15	0.90
Leaf-on 2023	477	1.52^{Aa}	0.86	1.20	0.91
Annual 2024	1429	1.63^{b}	0.71	1.18	0.91
Dormant 2024	804	1.56^{Cb}	0.78	1.19	0.91
Green-up 2024	182	1.78^{Db}	0.68	1.20	0.90
Leaf-on 2024	443	1.71^{Eb}	0.79	1.19	0.89

Note: superscript capital letters indicate significant differences among phenological phases within a given year, whereas superscript lowercase letters denote significant differences between years within the same phenological phase. For annual records, lowercase superscripts indicate significant difference between 2023 and 2024.

https://doi.org/10.5194/egusphere-2026-1635
Preprint. Discussion started: 8 April 2026

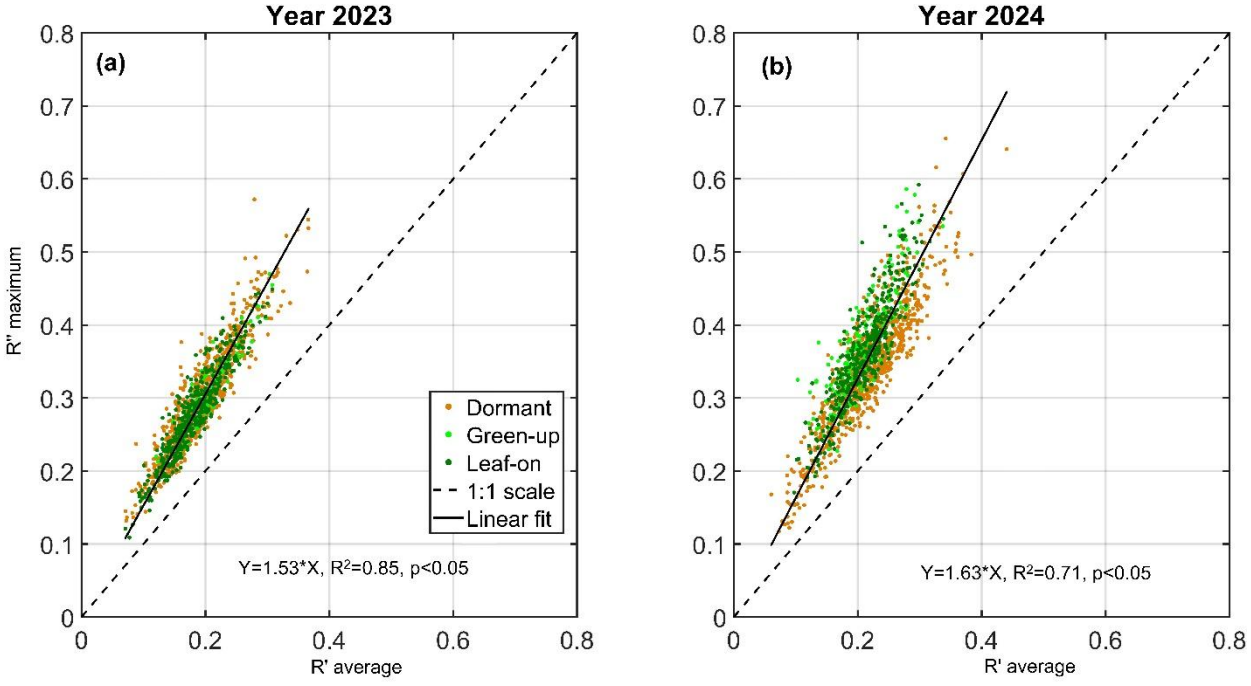

Figure 7. The relationship between the spatial average of R' and the corresponding spatial maximum R'' across all locations using all 5-min samples in a) 2023 and b) 2024. Different colors indicate phenological phases.

Linear regression analysis was repeated for 2024 using only data from sensors located at the same locations in both years across all phenological phases, thereby removing the potential influence of the additional eight locations installed in 2024 after the dormant phase. The resulting spatial variability of shear stress ratio for the three phases was 1.56, 1.77, and 1.69, respectively. The additional eight sensors contributed a negligible difference (less than 1.5 %) in spatial variability. Overall, the spatial variability of shear stress ratio in 2024 was 2-16 % higher than in 2023, suggesting locally enhanced erosivity. This interpretation was consistent with observed scouring near several Irwin locations (e.g., B3, B4, C3, C4, and D2 in supplementary Fig. S2) in 2024.

A significant linear relationship ($R^2 > 0.87$, $p < 0.05$) was found between R' and R'' at each sensor location. Temporal variability of shear stress ratio ranged from 1.15 to 1.29 and exhibited location-specific patterns, with larger values typically occurring at the furthest downwind positions (D and E locations, Fig. 1). On average, phenological transitions contributed less than a 3 % change in temporal variability in both years. For the same phenological phase across years, temporal variability was 3 % and 4 % higher in 2024 than in 2023 during the dormant and green-up phases, but 0.6 % lower in 2024 than in 2023 during the leaf-on phase. The eight additional sensors installed in 2024 altered temporal variability by less than 1.0 %, indicating a negligible effect. Across all locations, the average of temporal variability exceeded 1.137, the maximum value previously reported by King et al. (2006).

https://doi.org/10.5194/egusphere-2026-1635
Preprint. Discussion started: 8 April 2026

3.2 Spatial distribution of shear stress ratio

Overall, the interpolated R' patterns reflect the expected fluid acceleration along the side of the shrub, suggesting enhanced surface shear forcing (Fig. 8). Spatial distributions of R' varied among phenological phases, with consistently higher values in 2024 than in 2023 across all phases. The additional eight sensor locations in 2024 improved spatial resolution, especially in front of the shrub (AB1, B1, and ABB1.5) and along the side (B4 and D4). At AB1, located ~1h from the shrub's front edge, R' was less than 5.5 % lower than at the upwind reference point (3h from the front edge) during the green-up and leaf-on phases—periods when shrub morphology exerted the strongest influence. At ABB1.5, R' was 3.5 % lower than at AB1, likely reflecting the effect of deflected flow approaching the shrub. At B1, flow stagnation effects—such as pressure buildup, flow redirection, and localized turbulence—likely intensified with foliar development. For example, R' was 75.5 % of the reference value during green-up and increased to 88.5 % during leaf-on, indicating stronger stagnation during leaf-on conditions. At D4, R' was within 2 % of the reference location, a pattern not observed in 2023. With all 18 locations monitored in 2024, rows C and D formed a distinct high-R' plateau, suggesting an elevated potential for localized wind erosion.

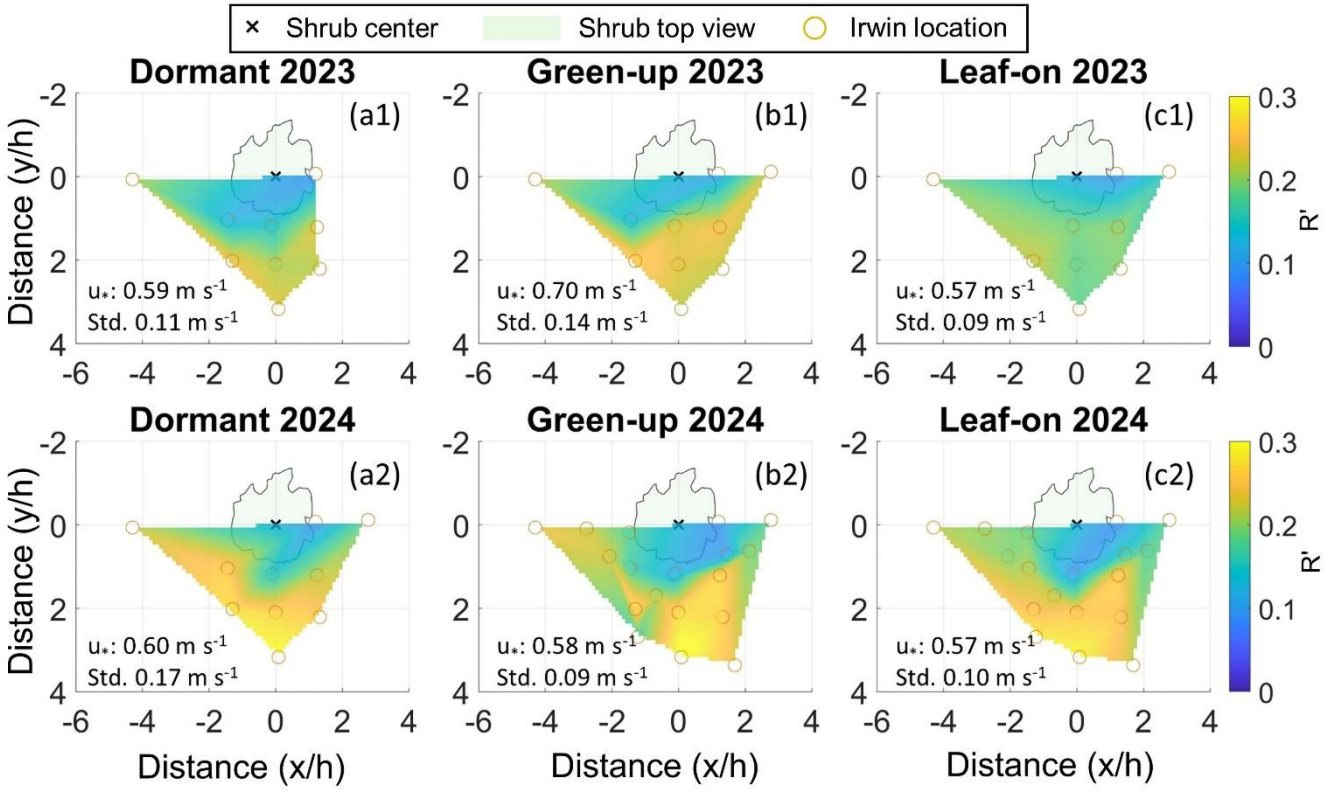

Figure 8. The spatial distribution of the linear interpolated R' during three phenological phases. The wind direction is from left to right.

https://doi.org/10.5194/egusphere-2026-1635
Preprint. Discussion started: 8 April 2026

3.3 Influence of wind speed and shrub phenology on shear stress ratio

Simple linear regression analyses were performed between R' and U, grouped by year and phenological phase. No statistically significant relationships were found between U and R' ($p < 0.05$, $R^2 > 0.1$). Regressions were repeated for each of the 18 individual locations to eliminate impacts from spatial averaging. Only two locations, both situated directly behind the shrub—D1 ($p < 0.05$, $R^2 = 0.11$) and E1 ($p < 0.05$, $R^2 = 0.23$)—showed a weak decreasing trend (slope = -0.015) in 2024. At C2, a significant negative relationship was observed during the 2024 leaf-on phase (slope = -0.03, $p < 0.05$, $R^2 = 0.37$), suggesting enhanced drag partitioning at higher U. Overall, R' around the shrub appeared independent of U across phenological phase (Fig. 9).

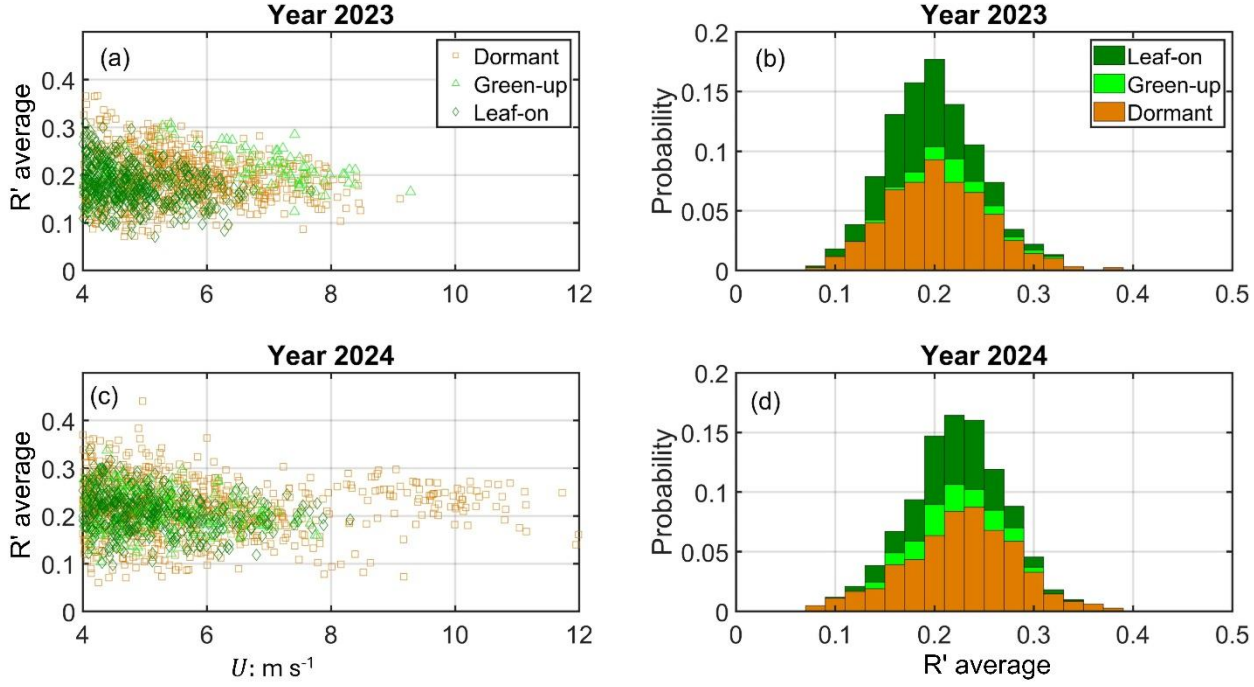

Figure 9. R' versus U at 1 m height for 2023 (a) and 2024 (c). Probability distribution of R' during dormant, green-up, and leaf-on phases in 2023 (b) and 2024 (d). No statistically significant relationship was found between R' and U for $p < 0.05$, $R^2 > 0.1$.

The percentage differences in R', i.e., $\Delta R'$, from the same locations between the dormant and leaf-on phases—when shrub morphology remains relatively stable—showed on average 11 % decrease in 2023 and 8 % decrease in 2024, except at two shrub-edge locations (C2: 33 % increase in 2023; D2: 20 % increase in 2024; Fig. 10a–b). The apparent upwind extension of increased $\Delta R'$ in 2023 is likely an interpolation artifact caused by missing data at location B2 (Fig. 10a). Significant decreases were observed at C4 in 2023 (–22 %) and at C2 in 2024 (–31 %). As shrub morphology and porosity changed with

https://doi.org/10.5194/egusphere-2026-1635
Preprint. Discussion started: 8 April 2026

phenology, $\Delta R'$ gradient steepened near the shrub edge, particularly between rows C and D (Fig. 9a–b), indicating increased erosion potential for positive $\Delta R'$.

From green-up to leaf-on in 2024, $\Delta R'$ significantly increased at three locations—B2 (+28 %), B4 (+66 %), and D1.5 (+54 %)—when all 18 sensors were operating simultaneously (Fig. 10c). The extreme increases were influenced by local scouring effects that elevated u_{*_s} estimates (B4), and by sensor malfunction (B2 and D1.5) identified after fieldwork in 2024. Excluding these outliers, R' decreased by an average of 5.7 % from green-up to leaf-on. Overall, phenological transitions led to increased R' around the shrub edge (Fig. 10), reflecting intensified wind forcing. These variations suggest that vegetation growth along the side channel may be constrained by enhanced wind forcing.

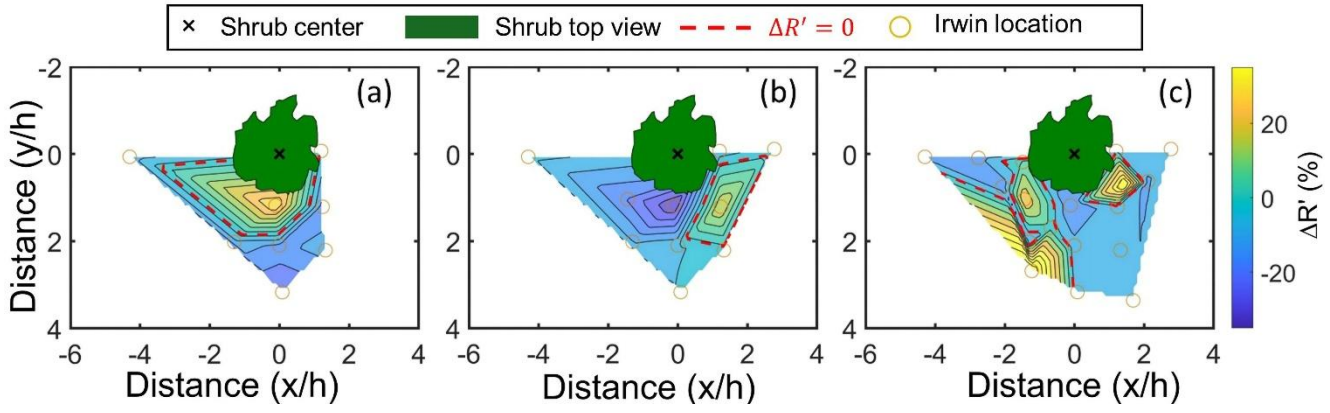

Figure 10. The percentage difference R' between phenological phases. (a) Dormant to leaf-on in 2023. (b) Dormant to leaf-on in 2024. (c) Green-up to leaf-on in 2024, based on all 18 sensors operating simultaneously. The dashed red line indicates zero difference in R'.

3.4 Patterns of erosivity, sheltering, and acceleration

The acceleration zone experiencing fluid acceleration (e >1) has a distinctive and irregular arcuate elliptical shape, extending from the shrub edge to ~2h outward (Fig. 11). The sheltering zone extended up to 1h from the shrub edge. In 2023, the separation line was ~1.0-1.5h from the shrub edge along rows B, C, and D during the dormant phase. As the green-up phase progressed, the area of the acceleration zone increased and shifted closer to the shrub along rows C and D. During the leaf-on phase, the acceleration zone retreated between rows D and E. The expansion along row B is likely an interpolation artifact caused by missing data at B2. In general, the highest erosivity value in 2023, 19 % higher than at A1 on average, occurred slightly upwind of the plant center at location B3.

In 2024, the erosivity values were notably higher, consistent with scouring observed near several locations (C4, B3, C3, D2) from March 8 through the end of the experiment (see supplementary Figs. S1 and S3). The separation line during the dormant phase resembled 2023, except near location B2, where a sensor malfunction occurred in 2024. During the green-up

https://doi.org/10.5194/egusphere-2026-1635
Preprint. Discussion started: 8 April 2026

phase, a small, isolated acceleration zone appeared at B3, possibly related to local scouring around the sensor, while the main acceleration zone developed farther downwind between rows C and D. By the leaf-on phase, a well-defined, arcuate elliptical shaped acceleration zone had formed. The highest erosivity value in 2024 occurred at C4, averaging 37 % higher than at A1.

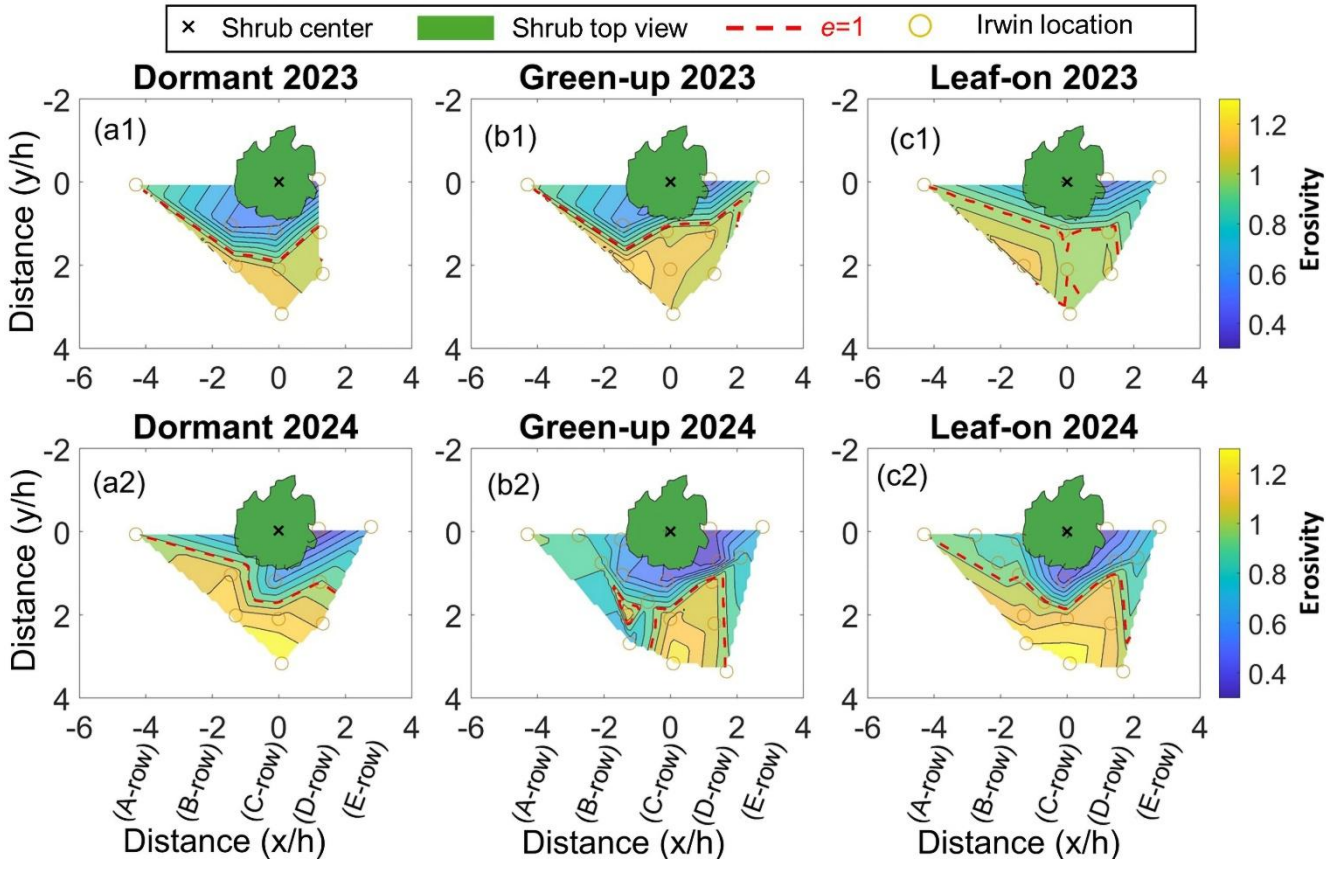

Figure 11. Spatial distribution of the linearly interpolated erosivity (e) during the three vegetation phenological phases. The dashed red line marks the $e = 1$ contour, separating shrub sheltering ($e < 1$) from acceleration ($e > 1$).

4 Discussion

This study shows how drag partitioning for a lateral shrub-interspace mosaic unit responds to varying wind forcing and vegetation phenological phases. The results provide a mechanistic basis for increased variability in wind erosion magnitude for a sparsely vegetated dryland and indicate phenology-dependent and wind forcing independent shear stress redistribution should be incorporated into next-generation drag partition formulations. Most prior research has focused on reductions in U or u_{*s} directly downwind of plants (e.g., Gillies et al., 2014; Mayaud et al., 2016b; Miri et al., 2017, 2018; Sutton & Neuman, 2008; Wu et al., 2013, and among many others), or on the distribution of U or u_{*s} for relatively short durations with static

https://doi.org/10.5194/egusphere-2026-1635
Preprint. Discussion started: 8 April 2026

phenology (Burri et al., 2011; Cheng et al., 2019; Fu et al., 2019; Leenders et al., 2007; Miri & Webb, 2022; Sutton & McKenna Neuman, 2008; Walter et al., 2012). To the best of our knowledge, no prior field studies have examined the spatial and temporal distribution of surface shear velocity on the side of an isolated vegetation element with such high measurement density and long duration. Understanding spatial patterns of u_{*_S} around vegetation elements and how they respond to changes in U and phenology is critical for understanding fundamental aeolian transport processes and flow-vegetation interactions such as drag partitioning in sparsely vegetated arid and semi-arid landscapes. Overall, our results demonstrate that the lateral acceleration zone is consistent with previous studies and that surface shear stress ratio (R') is independent of wind forcing and exhibited a statistically significant decrease trend with foliar growth, while maintaining pronounced spatial heterogeneity. Remaining uncertainties related to vegetation type and dimensional traits highlight important gaps in understanding the extent and shape of the acceleration zone.

4.1 Spatial and temporal variability of shear stress ratio

The spatial variability of R' in this study (1.49-1.78) is greater than previously reported values, which range from 1.03 to 1.41 (Crawley and Nickling, 2003; Kang et al., 2018; Walter et al., 2012). Given differences in scale, deployment, and vegetation from previous studies, our results are broadly comparable. Importantly, this study primarily characterized R' along the side of an isolated shrub, while previously published values reflect site-wide averages. Our results suggest that spatial variability of R' may be underestimated for the soil surface immediately adjacent to vegetation, which is where much of the aeolian sediment transport and net erosion occurs in sparsely vegetated landscapes (Breshears et al., 2009; Okin & Gillette, 2001; Okin, 2008; Ravi et al., 2007; Webb et al., 2020). However, Ziegler et al. (2023) showed a higher spatial variability of 2.28 (c.f. Fig. 9) derived from daily quantification of shear stress ratio measured in 27 randomly sampled locations over a 1 ha area. Using the same daily timescale, we found spatial variability of 2.21 and 2.43 in 2023 and 2024, respectively. These findings highlight the importance of temporal scale in evaluating the spatial variability of R', particularly in drylands where wind erosion is spatially heterogeneous and intermittent. Thus, appropriate spatial sampling and selecting an appropriate time scale is critical for practical uses of R', such as improving the accuracy of drag partition models.

Our estimates of temporal variability of R' range from 1.15 to 1.29 and exhibit location-specific patterns with maximum differences of 4 % in 2023 and 15 % in 2024. In general, temporal variability was larger at downstream than upstream locations. On average, temporal variability of R' from this study is 4 % higher than the value reported by King et al. (2006), which is reasonable given differences in sampling design. Across phenological phases, temporal variability was slightly higher during the leaf-on phase, with variation of less than 3 %. Results indicate that temporal variability varies by location but not strongly influenced by phenological transitions. On average, temporal variability was 77 % of the magnitude of spatial variability in 2023 and 72 % in 2024. These findings suggest that future research and wind erosion modeling efforts should explicitly incorporate both the spatial and temporal variability of R'.

https://doi.org/10.5194/egusphere-2026-1635
Preprint. Discussion started: 8 April 2026

4.2 Impacts of wind speed and phenology on shear stress ratio

Previous studies have shown that u_{*s} tends to increase with U (or u_*) in the sheltered zone behind vegetation (Gillies et al., 2014; Walter et al., 2012; Wolfe and Nickling, 1993). Here, on the side of an individual shrub, no significant relationship is detected between R' and U, regardless of phenological phase. At locations directly behind the shrub, a weak but statistically significant negative relationship between R' and U is observed in 2024 ($p < 0.05$), with fitted slope values of −0.015 at both D1 and E1 ($R^2 = 0.11$ and 0.23, respectively). At C2, situated at the shrub's lateral edge where the surface is directly sheltered, a stronger negative slope of −0.03 was detected during the 2024 leaf-on phase ($p < 0.05$; $R^2 = 0.37$). These results suggest that R' might decrease slightly with increasing U in the sheltered zone, implying a modest enhancement in the shrub's sheltering effect at higher U. However, this enhancement may come at the expense of reduced sheltering area extent. Other studies have shown that the zone with reduced U behind a plant tends to become more spatially concentrated closer to the vegetation as U increases (Miri, et al., 2017; Cheng et al., 2019). Further research is needed to better quantify how sheltering and its spatial extent vary with increasing U, and how these dynamics are controlled by vegetation characteristics.

More recently, Ziegler et al. (2023; Fig. 7) reported that average site-wide R' decreased 5 times with foliar growth. Here, R' along the shrub side also exhibited a statistically significant decreasing trend with growth, although the magnitude of decrease was only ~14 % (Fig. 5). However, the shear stress ratio was strongly heterogeneous, as indicated by the increasing trend in the spatial maximum R'' across phenological phases.

4.3 Acceleration zone comparison

Most studies examining acceleration along the side of vegetation have relied on wind speed measurements taken at various heights and locations beneath canopies or roughness elements (Ash and Wasson, 1983; Cheng et al., 2019; Leenders et al., 2007; Miri and Webb, 2022). However, the limitations of using height-dependent wind speed as a proxy for surface shear velocity are well documented (Bauer et al., 2013; Lee and Baas, 2016). A direct assessment is provided by Sutton and McKenna Neuman (2008), who measured surface shear stress around a wooden cylinder with equal height and diameter in a wind tunnel. Although they did not explicitly quantify the lateral acceleration zone's spatial extent, their Fig. 8(a) provides sufficient data to digitize the zone, enabling direct comparison with our field results. We compared our results to the synthesis of prior studies in Miri and Webb (2022) (Fig. 12). We used the acceleration zone observed during the 2024 leaf-on phase for comparison, when spatial measurement resolution was highest and foliage characteristics were best represented. A key distinction is that prior studies assumed or employed elements with equal height and crown diameter, whereas the shrub in our study has a crown diameter nearly twice its height.

https://doi.org/10.5194/egusphere-2026-1635
Preprint. Discussion started: 8 April 2026

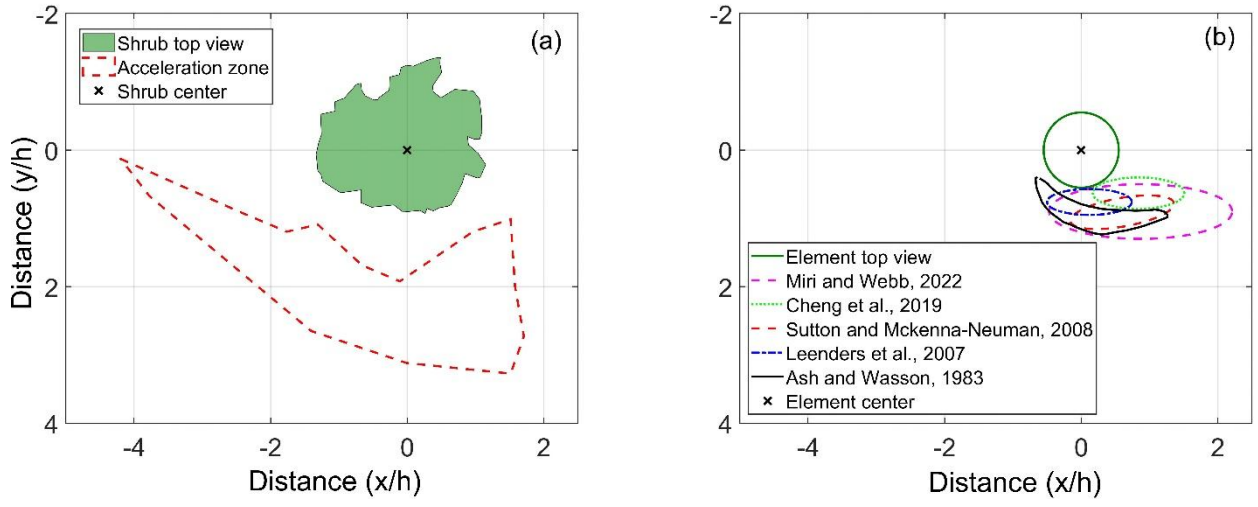

Figure 12. Comparison of the lateral acceleration features between this study (a) and previous studies (b). Both axes are normalized by the surface element height (h).

Qualitatively, our results show a similar acceleration zone to those reported by Ash and Wasson (1983) (Fig. 12(b)). However, the limited methodological detail in their study introduces uncertainty: wind speed was measured with a handheld anemometer, and neither measurement height nor vegetation characteristics were reported. As such, their delineation of the acceleration zone appears to be guided more by general observation than by systematically quantified field data. In contrast, the wind tunnel results of Sutton and McKenna Neuman (2008), based on direct surface shear stress measurements show an acceleration zone that originates near the lateral centerline and extends downwind. Differences between their results and ours likely reflect differences in surface element type, particularly their use of a solid wooden cylinder. The shrub in our study had a crown diameter nearly twice its height. Similar differences are also noted by Walter et al. (2012). Other acceleration zones observed using wind speed measurements generally display elliptical shapes but vary in extent and position. Notably, the relatively large acceleration zone reported by Miri and Webb (2022) may be attributed to the dense foliage of the 1.5 m tall shrub used in their study. Overall, the location and spatial distribution of lateral acceleration features appear to be strongly influenced by the dimensional characteristics of surface roughness elements. How these features vary across element types remains an open question. Numerical simulations by Fu et al. (2019), for example, demonstrated that acceleration effects are strongly controlled by element basal shape, underscoring the need for further investigation.

By quantifying R' characteristics, including its wind-independent and phenology-dependent responses and its spatial and temporal variability, this study builds a more complete two-dimensional view of wind–vegetation interactions in drylands. Incorporating our results into drag-partition schemes should improve predictions of the timing, location, magnitude, and frequency of aeolian sediment transport and dust emission, including low-intensity events when above-canopy winds are near or below conventional thresholds. Our results also underscore the geomorphic importance of acceleration zones around vegetation, where repeated scouring resulting from intensified saltation under higher wind shear velocities can abrade plant

https://doi.org/10.5194/egusphere-2026-1635
Preprint. Discussion started: 8 April 2026

tissues and expose roots, promoting plant mortality, canopy-gap expansion, and the formation of streets and nebkhas. In this way, we link small-scale flow–vegetation interactions to broader ecosystem transitions and landscape evolution. Results also highlight the importance of adequately sampling the spatial variability of aeolian sediment transport in studies to elucidate magnitude and change in wind erosion and dust emission rates (Webb et al., 2019; Wojcikiewicz et al., 2023).

5 Conclusions

This study presents the first detailed characterization of shear stress ratio (R') along the side of an isolated shrub in a sparsely vegetated rangeland, based on field data collected over 11 months including three phenological phases across two years. Results show that the spatial variability of R' was greater than that reported in earlier studies. The choice of temporal scale (e.g., daily versus minute resolution) is critical when quantifying spatial variability and, therefore, developing wind erosion and dust emission models. On average, temporal variability of R' was relatively small (<3 % difference across phenological phases), whereas spatial variability among locations reached up to 15 %. Overall, temporal variability was 75 % of the magnitude of spatial variability.

Along the shrub side, average R' declines significantly with foliar growth, yet the shear stress pattern remained highly heterogeneous, with localized areas of enhanced shear occurring near shrub margins. Observed R' was independent of wind speed. The R' response to wind forcing and phenology was nearly identical when analyzed over the narrower wind-direction range (245° ±10°) compared with the broader range (225° ±30°). Erosivity patterns further reveal that shrub sheltering could extend as far as approximately $1h$ from the edge along the side. The shape and position of the acceleration zone are broadly consistent with previous studies, though uncertainties remain regarding how vegetation type and dimensional traits influence its extent and shape.

Finally, we recognize that our findings are limited to a single shrub type, dimensional scale, and foliar porosity variation. Future work could examine how lateral shear velocity responds to variations in vegetation shape and scaling across plant types. Addressing this knowledge gap will improve soil erosion prediction by incorporating the lateral acceleration of wind around vegetation into drag-partition schemes, leading to more realistic estimates of surface shear stress. More accurate predictions of where and when erosion occurs can inform rangeland management strategies aimed at reducing vegetation loss and stabilizing soils. This is especially critical in sparsely vegetated drylands, where limited canopy cover magnifies the influence of acceleration zones and small changes in vegetation structure can disproportionately affect landscape stability.

Data availability

The data that support the findings of this study are openly available in Zenodo at https://doi.org/10.5281/zenodo.17178745

https://doi.org/10.5194/egusphere-2026-1635
Preprint. Discussion started: 8 April 2026

Supplementary material

The supplementary photographs show scouring features resulting from wind erosion, supporting enhanced erosion along the shrub side.

Author contributions

Conceptualization: Pei Zhang, Brandon L. Edwards, John A. Gillies, Nancy P. Zeigler
Data curation: Pei Zhang, Brandon L. Edwards
Formal analysis: Pei Zhang
Funding acquisition: Andrew Trautz, Nancy P. Ziegler
Investigation: Pei Zhang, Brandon L. Edwards
Methodology: Pei Zhang, Brandon L. Edwards, John A. Gillies, George Nikolich, Andrew Trautz, Brandi Wheeler, Nancy P. Ziegler
Project administration: Brandon L. Edwards
Supervision: Brandon L. Edwards, Andrew Trautz, Nancy P. Zeigler
Validation: Pei Zhang, Brandon L. Edwards
Visualization: Pei Zhang
Writing – original draft: Pei Zhang
Writing – review & editing: Pei Zhang, Brandon L. Edwards, John A. Gillies, George Nikolich, Andrew Trautz, Brandi Wheeler, Nancy P. Ziegler

Competing interests

The authors declare that they have no conflict of interest.

Acknowledgements

This research was a contribution of the Long-Term Agroecosystem Research (LTAR) network supported by the U.S. Department of Agriculture (USDA). This work was also supported by USACE agreement #472-3050-078. Nicholas Webb and Justin Van Zee were disapproved of authorship following USDA policy. Nicholas Webb contributed Conceptualization, Funding acquisition, Resources, Methodology, Investigation, Project administration, Supervision, and Writing - review and editing. Justin Van Zee contributed Methodology, Investigation, Resources, and Writing - review and editing.

Vegetation phenology data used in this research were provided by the PhenoCam Network, which has been supported by the National Science Foundation, the Long-Term Agroecosystem Research (LTAR) network which is supported by the United

https://doi.org/10.5194/egusphere-2026-1635
Preprint. Discussion started: 8 April 2026

States Department of Agriculture (USDA), the U.S. Department of Energy, the U.S. Geological Survey, the Northeastern States Research Cooperative, and the USA National Phenology Network. We thank the PhenoCam Network collaborators, including site PIs and technicians, for publicly sharing the data that were used in this paper.

References

Ash, J. E. and Wasson, R. J.: Vegetation and sand mobility in the Australian desert dunefield., Zeitschrift fur Geomorphologie, Supplementband, 45, 1983.

Baas, A. C. W.: Grains in Motion, in: Aeolian Geomorphology, Wiley, 27–60, https://doi.org/10.1002/9781118945650.ch2, 2019.

Bauer, B. O., Walker, I. J., Baas, A. C. W., Jackson, D. W. T., Neuman, C. M. K., Wiggs, G. F. S., and Hesp, P. A.: Critical Reflections on the Coherent Flow Structures Paradigm in Aeolian Geomorphology, in: Coherent Flow Structures at Earth's Surface, https://doi.org/10.1002/9781118527221.ch8, 2013.

Bauer, B. O., Hesp, P. A., Smyth, T. A. G., Walker, I. J., Davidson-Arnott, R. G. D., Pickart, A., Grilliot, M., and Rader, A.: Air flow and sediment transport dynamics on a foredune with contrasting vegetation cover, Earth Surf. Process. Landf., 47, https://doi.org/10.1002/esp.5425, 2022.

Bergametti, G. and Gillette, D. A.: Aeolian sediment fluxes measured over various plant/soil complexes in the Chihuahuan desert, J. Geophys. Res. Earth Surf., 115, https://doi.org/10.1029/2009JF001543, 2010.

van Boxel, J. H., Sterk, G., and Arens, S. M.: Sonic anemometers in aeolian sediment transport research, Geomorphology, 59, https://doi.org/10.1016/j.geomorph.2003.09.011, 2004.

Breshears, D. D., Whicker, J. J., Zou, C. B., Field, J. P., and Allen, C. D.: A conceptual framework for dryland aeolian sediment transport along the grassland-forest continuum: Effects of woody plant canopy cover and disturbance, Geomorphology, 105, https://doi.org/10.1016/j.geomorph.2007.12.018, 2009.

Burkey, J.: Mann-Kendall Tau-b with Sen's Method (enhanced), https://www.mathworks.com/matlabcentral/fileexchange/11190-mann-kendall-tau-b-with-sen-s-method-enhanced/files/ktaub.m, 2020.

Burri, K., Gromke, C., Lehning, M., and Graf, F.: Aeolian sediment transport over vegetation canopies: A wind tunnel study with live plants, Aeolian Res., 3, https://doi.org/10.1016/j.aeolia.2011.01.003, 2011.

Chappell, A., McTainsh, G., Leys, J., and Strong, C.: Using geostatistics to elucidate temporal change in the spatial variation of aeolian sediment transport, Earth Surf. Process. Landf., 28, https://doi.org/10.1002/esp.463, 2003.

Cheng, H., He, W., Liu, C., Zou, X., Kang, L., Chen, T., and Zhang, K.: Transition model for airflow fields from single plants to multiple plants, Agric. For. Meteorol., 266–267, https://doi.org/10.1016/j.agrformet.2018.11.039, 2019.

Crawley, D. M. and Nickling, W. G.: Drag partition for regularly-arrayed rough surfaces, Boundary. Layer. Meteorol., 107, https://doi.org/10.1023/A:1022119909546, 2003.

https://doi.org/10.5194/egusphere-2026-1635
Preprint. Discussion started: 8 April 2026

Duniway, M. C., Pfennigwerth, A. A., Fick, S. E., Nauman, T. W., Belnap, J., and Barger, N. N.: Wind erosion and dust from US drylands: a review of causes, consequences, and solutions in a changing world, Ecosphere, 10, https://doi.org/10.1002/ecs2.2650, 2019.

Dupont, S., Bergametti, G., and Simoëns, S.: Modeling aeolian erosion in presence of vegetation, J. Geophys. Res. Earth Surf., 119, 168–187, https://doi.org/10.1002/2013JF002875, 2014.

Etyemezian, V., Gillies, J. A., Shinoda, M., Nikolich, G., King, J., and Bardis, A. R.: Accounting for surface roughness on measurements conducted with PI-SWERL: Evaluation of a subjective visual approach and a photogrammetric technique, Aeolian Res., 13, https://doi.org/10.1016/j.aeolia.2014.03.002, 2014.

Fu, L. T.: Comparisons suggest more efforts are required to parameterize wind flow around shrub vegetation elements for predicting aeolian flux, Sci. Rep., 9, https://doi.org/10.1038/s41598-019-40491-z, 2019.

Fu, L. T., Fan, Q., and Huang, Z. L.: Wind speed acceleration around a single low solid roughness in atmospheric boundary layer, Sci. Rep., 9, https://doi.org/10.1038/s41598-019-48574-7, 2019.

Gillette, D. A., Herrick, J. E., and Herbert, G. A.: Wind characteristics of Mesquite Streets in the northern Chihuahuan Desert, New Mexico, USA, Environmental Fluid Mechanics, 6, https://doi.org/10.1007/s10652-005-6022-7, 2006.

Gillies, J. A., Nickling, W. G., and King, J.: Aeolian sediment transport through large patches of roughness in the atmospheric inertial sublayer, J. Geophys. Res. Earth Surf., 111, https://doi.org/10.1029/2005JF000434, 2006.

Gillies, J. A., Nickling, W. G., and King, J.: Shear stress partitioning in large patches of roughness in the atmospheric inertial sublayer, Boundary. Layer. Meteorol., 122, https://doi.org/10.1007/s10546-006-9101-5, 2007.

Gillies, J. A., Nield, J. M., and Nickling, W. G.: Wind speed and sediment transport recovery in the lee of a vegetated and denuded nebkha within a nebkha dune field, Aeolian Res., 12, https://doi.org/10.1016/j.aeolia.2013.12.005, 2014.

Hong, C., Chenchen, L., Xueyong, Z., Huiru, L., Liqiang, K., Bo, L., and Jifeng, L.: Wind erosion rate for vegetated soil cover: A prediction model based on surface shear strength, Catena (Amst)., 187, https://doi.org/10.1016/j.catena.2019.104398, 2020.

Judd, M. J., Raupach, M. R., and Finnigan, J. J.: A wind tunnel study of turbulent flow around single and multiple windbreaks, part I: Velocity fields, Boundary. Layer. Meteorol., 80, https://doi.org/10.1007/BF00119015, 1996.

Kang, L., Zhang, J., Yang, Z., Zou, X., Cheng, H., and Zhang, C.: Experimental Investigation on Shear-Stress Partitioning for Flexible Plants with Approximately Zero Basal-to-Frontal Area Ratio in a Wind Tunnel, Boundary. Layer. Meteorol., 169, 251–273, https://doi.org/10.1007/s10546-018-0373-3, 2018.

King, J., Nickling, W. G., and Gillies, J. A.: Representation of vegetation and other nonerodible elements in aeolian shear stress partitioning models for predicting transport threshold, J. Geophys. Res. Earth Surf., 110, https://doi.org/10.1029/2004JF000281, 2005.

King, J., Nickling, W. G., and Gillies, J. A.: Aeolian shear stress ratio measurements within mesquite-dominated landscapes of the Chihuahuan Desert, New Mexico, USA, Geomorphology, 82, 229–244, https://doi.org/10.1016/j.geomorph.2006.05.004, 2006.

https://doi.org/10.5194/egusphere-2026-1635
Preprint. Discussion started: 8 April 2026

King, J., Nickling, W. G., and Gillies, J. A.: Investigations of the law-of-the-wall over sparse roughness elements, J. Geophys. Res. Earth Surf., 113, https://doi.org/10.1029/2007JF000804, 2008.

Kunadi, A. S., Silberstein, R. P., and Thompson, S. E.: Variation in Zero Plane Displacement and Roughness Length for Momentum Revisited, Boundary. Layer. Meteorol., 190, 36, https://doi.org/10.1007/s10546-024-00876-8, 2024.

de Langre, E.: Effects of wind on plants, https://doi.org/10.1146/annurev.fluid.40.111406.102135, 2008.

Lee, Z. S. and Baas, A. C. W.: Variable and conflicting shear stress estimates inside a boundary layer with sediment transport, Earth Surf. Process. Landf., 41, 435–445, 2016.

Leenders, J. K., Boxel, J. H. van, and Sterk, G.: The effect of single vegetation elements on wind speed and sediment transport in the Sahelian zone of Burkina Faso, Earth Surf. Process. Landf., 32, 1454–1474, https://doi.org/10.1002/esp.1452, 2007.

Li, J., Okin, G. S., Alvarez, L., and Epstein, H.: Effects of wind erosion on the spatial heterogeneity of soil nutrients in two desert grassland communities, Biogeochemistry, 88, https://doi.org/10.1007/s10533-008-9195-6, 2008.

Mayaud, J. and Webb, N.: Vegetation in Drylands: Effects on Wind Flow and Aeolian Sediment Transport, Land (Basel)., 6, 64, https://doi.org/10.3390/land6030064, 2017.

Mayaud, J. R., Wiggs, G. F. S., and Bailey, R. M.: Characterizing turbulent wind flow around dryland vegetation, Earth Surf. Process. Landf., 41, https://doi.org/10.1002/esp.3934, 2016a.

Mayaud, J. R., Wiggs, G. F. S., and Bailey, R. M.: Dynamics of skimming flow in the wake of a vegetation patch, Aeolian Res., 22, https://doi.org/10.1016/j.aeolia.2016.08.001, 2016b.

McKenna Neuman, C. and Bédard, O. O.: A wind tunnel study of flow structure adjustment on deformable sand beds containing a surface-mounted obstacle, J. Geophys. Res. Earth Surf., 120, https://doi.org/10.1002/2015JF003475, 2015.

Miri, A. and Webb, N. P.: Characterizing the spatial variations of wind velocity and turbulence intensity around a single Tamarix tree, Geomorphology, 414, https://doi.org/10.1016/j.geomorph.2022.108382, 2022.

Miri, A., Dragovich, D., and Dong, Z.: Vegetation morphologic and aerodynamic characteristics reduce aeolian erosion, Sci. Rep., 7, https://doi.org/10.1038/s41598-017-13084-x, 2017.

Miri, A., Dragovich, D., and Dong, Z.: The response of live plants to airflow – Implication for reducing erosion, Aeolian Res., 33, https://doi.org/10.1016/j.aeolia.2018.06.002, 2018.

Okin, G. and Gillette, D. A.: Distribution of vegetation in wind-dominated landscapes: Implications for wind erosion modeling and landscape processes, Journal of Geophysical Research: Atmospheres, 106, 9673–9683, https://doi.org/10.1029/2001JD900052, 2001.

Okin, G. S.: A new model of wind erosion in the presence of vegetation, J. Geophys. Res. Earth Surf., 113, https://doi.org/10.1029/2007JF000758, 2008.

Payne, S. A. R., Okin, G. S., Bhattachan, A., and Fischella, M. R.: The two faces of Janus: Processes can be both exogenous forcings and endogenous feedbacks with wind as a case study, Ecology, 104, https://doi.org/10.1002/ecy.3998, 2023.

https://doi.org/10.5194/egusphere-2026-1635
Preprint. Discussion started: 8 April 2026

PhenoCam Network: PhenoCam Data for Jernwern SH_1000, available at https://phenocam.nau.edu/webcam/roi/jernwern/SH_1000/ , accessed January 2023 to July 2024., 2024.

Raupach, M. R.: Drag and drag partition on rough surfaces, Boundary. Layer. Meteorol., 60, https://doi.org/10.1007/BF00155203, 1992.

Raupach, M. R., Gillette, D. A., and Leys, J. F.: The effect of roughness elements on wind erosion threshold, J. Geophys. Res., 98, https://doi.org/10.1029/92JD01922, 1993.

Ravi, S., D'Odorico, P., and Okin, G. S.: Hydrologic and aeolian controls on vegetation patterns in arid landscapes, Geophys. Res. Lett., 34, https://doi.org/10.1029/2007GL031023, 2007.

Richardson, A. D., Hufkens, K., Milliman, T., and Frolking, S.: Intercomparison of phenological transition dates derived from the PhenoCam Dataset V1.0 and MODIS satellite remote sensing, Sci. Rep., 8, 5679, https://doi.org/10.1038/s41598-018-23804-6, 2018.

Shaw, R. H.: Secondary wind speed maxima inside plant canopies., J APPL. METEOROL., 16, https://doi.org/10.1175/1520-0450(1977)016<0514:swsmip>2.0.co;2, 1977.

Sterk, G., Stein, A., and Stroosnijder, L.: Wind effects on spatial variability in pearl millet yields in the Sahel, Soil Tillage Res., 76, https://doi.org/10.1016/j.still.2003.08.004, 2004.

Suter-Burri, K., Gromke, C., Leonard, K. C., and Graf, F.: Spatial patterns of aeolian sediment deposition in vegetation canopies: Observations from wind tunnel experiments using colored sand, Aeolian Res., 8, https://doi.org/10.1016/j.aeolia.2012.11.002, 2013.

Sutton, S. L. F. and McKenna-Neuman, C.: Variation in bed level shear stress on surface sheltered by nonerodible roughness elements, J. Geophys. Res. Earth Surf., 113, https://doi.org/10.1029/2007JF000967, 2008.

Sutton, S. L. F. and Neuman, C. M. K.: Sediment entrainment to the lee of roughness elements: Effects of vortical structures, J. Geophys. Res. Earth Surf., 113, https://doi.org/10.1029/2007JF000783, 2008.

Walter, B., Gromke, C., Leonard, K. C., Manes, C., and Lehning, M.: Spatio-Temporal Surface Shear-Stress Variability in Live Plant Canopies and Cube Arrays, Boundary. Layer. Meteorol., 143, https://doi.org/10.1007/s10546-011-9690-5, 2012.

Webb, N. P., Herrick, J. E., Van Zee, J. W., Courtright, E. M., Hugenholtz, C. H., Zobeck, T. M., Okin, G. S., Barchyn, T. E., Billings, B. J., Boyd, R., Clingan, S. D., Cooper, B. F., Duniway, M. C., Derner, J. D., Fox, F. A., Havstad, K. M., Heilman, P., LaPlante, V., Ludwig, N. A., Metz, L. J., Nearing, M. A., Norfleet, M. L., Pierson, F. B., Sanderson, M. A., Sharratt, B. S., Steiner, J. L., Tatarko, J., Tedela, N. H., Toledo, D., Unnasch, R. S., Van Pelt, R. S., and Wagner, L.: The National Wind Erosion Research Network: Building a standardized long-term data resource for aeolian research, modeling and land management, Aeolian Res., 22, https://doi.org/10.1016/j.aeolia.2016.05.005, 2016.

Webb, N. P., Chappell, A., Edwards, B. L., McCord, S. E., Van Zee, J. W., Cooper, B. F., Courtright, E. M., Duniway, M. C., Sharratt, B., Tedela, N., and Toledo, D.: Reducing Sampling Uncertainty in Aeolian Research to Improve Change Detection, J. Geophys. Res. Earth Surf., 124, https://doi.org/10.1029/2019JF005042, 2019.

https://doi.org/10.5194/egusphere-2026-1635
Preprint. Discussion started: 8 April 2026

595 Webb, N. P., Okin, G. S., Bhattachan, A., D'Odorico, P., Dintwe, K., and Tatlhego, M.: Ecosystem dynamics and aeolian sediment transport in the southern Kalahari, Afr. J. Ecol., 58, https://doi.org/10.1111/aje.12700, 2020.

Webb, N. P., Wheeler, B., Edwards, B. L., Schallner, J. W., Macanowicz, N., Van Zee, J. W., Courtright, E. M., Cooper, B., McCord, S. E., Browning, D., Dhital, S., Young, K. E., and Bestelmeyer, B. T.: Magnitude Shifts in Aeolian Sediment Transport Associated With Degradation and Restoration Thresholds in Drylands, J. Geophys. Res. Biogeosci., 130,
600 https://doi.org/10.1029/2024JG008581, 2025.

Wojcikiewicz, R. R. K., Webb, N. P., Edwards, B. L., Van Zee, J. W., Courtright, E. M., Cooper, B. F., and Hanan, N. P.: Aeolian Sediment Transport Responses to Vegetation Cover Change: Effects of Sampling Error on Model Uncertainty, J. Geophys. Res. Earth Surf., 128, https://doi.org/10.1029/2023JF007319, 2023.

Wolfe, S. A. and Nickling, W. G.: The protective role of sparse vegetation in wind erosion, Prog. Phys. Geogr., 17,
605 https://doi.org/10.1177/030913339301700104, 1993.

Wu, T., Yu, M., Wang, G., Wang, Z., Duan, X., Dong, Y., and Cheng, X.: Effects of stand structure on wind speed reduction in a Metasequoia glyptostroboides shelterbelt, Agroforestry Systems, 87, https://doi.org/10.1007/s10457-012-9540-6, 2013.

Zhang, P., Edwards, B. L., Webb, N. P., Trautz, A., Gillies, J. A., Ziegler, N. P., and Van Zee, J. W.: An evaluation of different
610 approaches for estimating shear velocity in aeolian research studies, Aeolian Res., 70–71, 100945, https://doi.org/10.1016/j.aeolia.2024.100945, 2024.

Zhang, P., Edwards, B., Gillies, J., Nikolich, G., Trautz, A., Wheeler, B., and Ziegler, N.: Data for: The Spatial Distribution of Surface Wind Shear Velocity Around a Shrub in a Sparsely Vegetated Dryland, Data set, 2025.

Ziegler, N. P., Webb, N. P., Gillies, J. A., Edwards, B. L., Nikolich, G., Van Zee, J. W., Cooper, B. F., Browning, D. M.,
615 Courtright, E. M., and LeGrand, S. L.: Plant phenology drives seasonal changes in shear stress partitioning in a semi-arid rangeland, Agric. For. Meteorol., 330, 109295, https://doi.org/10.1016/j.agrformet.2022.109295, 2023.

Ziegler, N. P., Webb, N. P., Edwards, B. L., Nikolich, G., Gillies, J. A., Patel, S. G., Wheeler, B., Zhang, P., Van Zee, J. W., LeGrand, S. L., and Trautz, A. C.: An updated Irwin sensor for measurement of surface shear velocity, Aeolian Res., 75, 101024, https://doi.org/10.1016/j.aeolia.2025.101024, 2026.

620